ISSN (Print) 1226-1750
ISSN (Online) 2233-6656
Journal of Magnetics 22(1), 69-77 (2017) https://doi.org/10.4283/JMAG.2017.22.1.069

Parametric Optimization and Performance Analysis of Outer Rotor Permanent Magnet Flux Switching Machine for Downhole Application

Rajesh Kumar*, Erwan Sulaiman, Mahyuzie Jenal, and Fatiah Shafiqah Bahrim

Research Center for Applied Electromagnetics, University of Tun Hussein Onn Malaysia, Locked Bag 101, Parit Raja, Batu Pahat, Johor, Malaysia

(Received 25 January 2017, Received in final form 21 February 2017, Accepted 23 February 2017)

To empower safe, economical and eco-friendly sustainable solution for enhancing oil and gas productivity from deep water reservoirs, new downhole technologies are recommended. Since electric machine plays leading role in the downhole application, it is a squeezing requirement for researchers to design and develop advanced electric machine. The Recent improvement in technology and uses of high-temperature magnets, permanent magnet flux switching machine (PMFSM) has become one of the appropriate contenders for offshore drilling but fewer designed for downhole due to ambient temperature. Therefore this comprehensive study deals with the design optimization and performance analysis of outer rotor PMFSM for the downhole application. Preliminary, the basic design parameters needed for machine design are calculated mathematically. Then the design refinement technique is implemented through deterministic method. Finally, initial and optimized performance of the machine is compared and as a result the output torque is increase from 16.39 Nm to 33.57 Nm while diminishing the cogging torque and PM weight up to 1.77 Nm and 0.79 kg, respectively. Therefore, it is concluded that purposed optimized design is suitable for the downhole application.

Keywords : downhole application, flux switching, optimization, outer rotor, permanent magnet

1. Introduction

Energy is the main thrust of the worldwide economy. Fig. 1 demonstrates the anticipated energy prerequisite from various resources to guarantee the improvement of the global economy from now to 2035 [1]. The majority of the increased production of oil and gas in coming decades is from the following two sources.

(i) Mature Fields

(ii) Deep Water Reservoirs

These mature fields today represent more than 70 % of the overall oil and gas production. The generation is gradually declining and the fields will be closed down rashly if the advance technology for enhancing recuperation financially savvy operation and support are not set up [2]. The worldwide oil and gas chase for new oil and gas assets is driving us into ever more profound waters and harsher environment. The most effective method to endeavor more oil and gas resources in the deepwater and

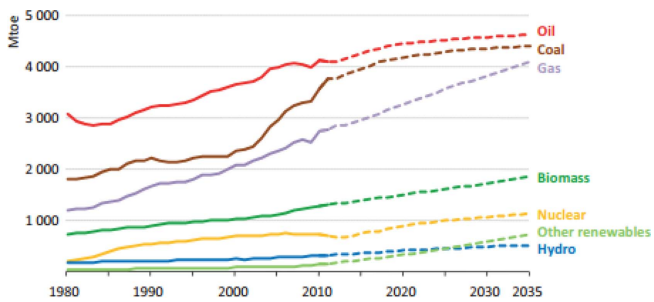

Fig. 1. (Color online) Global energy consumption [1].

develop them in a protected, proficient and all the more ecological way is a challenge. The cost of customarily settled or drifting platforms for processing, which are today generally utilized increases significantly in light of the fact that the stages are exceptionally costly to install and fabricate and for the fixed platforms demounting also costs hundreds of millions dollars afterward. With the traditional technologies, numerous deepwater fields are uneconomical to develop.

Downhole processing, by moving the processing from topside or inland to downhole can not just take out the top stages or somewhat diminish the top territory, but also

©The Korean Magnetics Society. All rights reserved.
*Corresponding author: Tel: +60197660121
Fax: +6074536060, e-mail: rajeshkumar@iiee.edu.pk

© 2017 Journal of Magnetics

generally improve production, extreme recuperation and preparing productivity while diminishing ecological effects [4].

An electric machine is the core of downhole application because more than 30 % of electrical system failure occurs in the machine shown in Table 1 [5]. The machine must bear the qualities of high reliability, better efficiency, high torque density and easy control. The present standard electrical downhole machine is induction machine which is moderately inefficient. Furthermore, the characteristic shortcoming of low starting torque and high starting current limits induction machine to low-torque, high-speed applications. In applications where high torque is needed, a mechanical gear is regularly added to coordinate the torque, this not just further diminishing the framework efficiency, likewise, debases the framework unwavering quality [6]. On the other hand, permanent magnet (PM) machines having higher efficiencies, higher torque densities and littler volumes, are generally utilized in modern applications to supplant traditional machines, however few have been produced for the downhole applications because of the high atmospheric temperatures in profound wells and the low-temperature stability of PM materials over the time. Today, with the improvement of cutting edge innovations and utilizations of high-temperature magnets, it is progressively fascinating for oil and gas businesses to create PM machines for the downhole applications [7]. A permanent magnet direct current (PMDC) downhole machine has been proposed for the downhole application. The direct current is effortlessly transmitted through PMDC to downhole by decreasing the transmission losses. It is easy to control because it does not require variable frequency drive (VFD). Notwithstanding, it has a couple of downsides, for example, the commutator system in PMDC not only introduces the complexity in assembling, additional losses over the brushes and also causes frequent failure. Furthermore, regular replacement is required every 2-3 years [8]. In order to overcome the problem of brushes, a brushless interior permanent magnet machine (IPM) was developed but it requires additional cooling facility [9].

The permanent magnet flux switching machine (PMFSM) has a brief history and is a moderately new sort of PM machines. The primary PMFSM was accounted for as a solitary phase alternator in 1955 using a low execution magnet depicted in Fig. 2(a), while a three-phase machine was presented in 1997 where ferrite was embraced to observe the flux centering impact appeared in Fig. 2(b) [10, 11]. More recently, there have been revived research interests in PMFSM, most likely because of number of saw advantages. Since all active parts such as armature windings and PM placed on the stator, straightforward yet viable machine cooling can be effortlessly connected [12]. Besides, extra preferences such as robust rotor structure, high torque and flux densities, high efficiency and better flux weakening capability are exhaustively analyzed and checked for numerous applications [13-15].

Setting the rotor on the external surface will produce more torque, contrasted with the routine internal rotor [16]. However, investigation on the PMFSM has, for the most part, centered on the electromagnetic examination and optimization of the inward rotor type machines with scarcely gave careful consideration to the external rotor PMFSM [17-19].

This paper primarily focused on design and optimization outer rotor PMFSM for the downhole application. Firstly, design key parameters are derived by utilizing mathematical formulas then it is modeled and simulated on 2D-FEA Finite Element Analysis (FEA) package, JMAG-Designer ver.14.0. The purposed design is unable to produce torque of 25 Nm. Therefore, the machine is optimized through the deterministic approach where design free parameters are adjusted in order to enhance the output of the machine. Finally, the performance comparison of initial and improved design is carried out in the last section.

Table 1. Component failure in ESP system for the downhole application [5].

Components	Failure Percentage
Assembly	1
Cable	21
Sensor	1
Pump	30
Gas Handler	1
Motor	32
Intake	4
Protector	10
Other	1

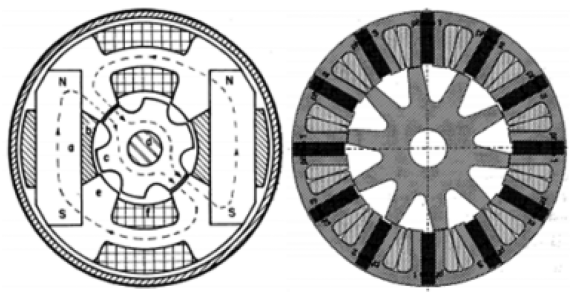

(a) (b)

Fig. 2. (a) Single phase alternator (b) Three phase brushless machine.

2. Geometric Topology

The basic design parameters are constrained by geometric relationship, interpreted in a magnified local structure shown in Fig. 3(a). The stator slot ought to be even multiple of phase numbers. In this manner, the relationship between stator slot number and N_s rotor pole number N_r is [20]

$$N_r = \frac{(12 \pm n) \times N_s}{6} \tag{1}$$

where n is a positive whole number which ought not to be multiple of three. In order to achieve zero resultant magnetic force, N_r is chosen to be an even number. The key outline parameters such as stator tooth arc width β_s, rotor pole arc width β_r, permanent magnet arc width βpm and stator armature slot width arc β_{slot} preliminary fixed as

$$\beta_r = \beta_s = \beta_{pm} = \frac{\beta_{slot}}{3} = \frac{\pi}{3N_s} \tag{2}$$

Simultaneously, the additional relationship between stator inner radius R_{si}, and outer radius R_{so}, stator back length h_{ys} and rotor yoke length h_{yr} are originally settled at

$$R_{si} = \frac{R_{so}}{2} \tag{3}$$

$$h_{yr} = 1.5 \times h_{ys} \tag{4}$$

Therefore, ratio between stator inner radius and stator outer radius is 0.5. Moreover, to get adequate rotor saliency, the rotor pole height h_{pr} is set as

$$h_{pr} = \frac{R_{so}}{8} \tag{5}$$

In addition, stator slot winding area A_{slot} can be resolved as

$$A_{slot} = \frac{R_{so}^2 \times \sin\left(\frac{\pi}{2N_s}\right)^2}{2\tan\left(\frac{\pi}{N_s}\right)} \tag{6}$$

Furthermore, number of turns N_a for one stator slot and peak injected current I_m in each coil can be determined as

$$N_a = \frac{2A_{slot} \times \alpha}{\pi d^2} \tag{7}$$

$$I_m = \frac{Ja \times A_{slot} \times \alpha}{2N_a} \tag{8}$$

where, α is filling component, d is the diameter of wire and Ja is the peak injected current density. At last, the rotor outer radius can be derived as

$$R_{ro} = \left(\frac{9}{8} + \frac{\pi}{2N_s}\right) \times R_{so} + g \tag{9}$$

Table 2. Specifications of initial outer rotor PMSFM for the downhole application.

Parameters	Abbreviation	Value	Units
Stator slot number	N_s	12	
Rotor pole number	N_r	22	
Rotor outer radius	R_{ro}	50	mm
Rotor inner radius	R_{ri}	40.5	mm
Stator inner radius	R_{si}	20	mm
Stator outer radius	R_{so}	40	mm
Stator back length	h_{ys}	3	mm
Rotor yoke length	h_{yr}	4.5	mm
Rotor pole arc width	β_r	5	°
Stator tooth arc width	β_s	5	°
Permanent magnet arc width	β_{pm}	5	°
Slot area	A_{slot}	50.732	mm^2
Air gap	g	0.5	mm
Stack length	l	200	mm
Number of Turns	N_a	33	
Synchronous speed	ω	1000	rpm
Armature current density	Ja	30	A/mm^2
Split ratio	λ	0.8	
Permanent Magnet Weight	W_{pm}	1.26	kg

where, g is the air gap. The complete schematic of proposed design is depicted in Fig. 3(b) is developed by key geometric parameters of outer rotor PMFSM shown in Table 2, that are ascertained through above mentioned equations.

3. Optimization

Preliminary, the performance of proposed machine design is computed through 2D-FEA, yet the objective torque is not accomplished for the downhole application. To handle this issue, design free parameters, L1 to L7 defined in rotor and stator sides as illustrated in Fig. 4, optimized through deterministic technique. The deterministic method is utilized to locate the greatest execution of machine by changing the design free parameters while keeping the air gap constant. The flow chart of the deterministic method is depicted in Fig. 5. Basically, the design parameters are classified into groups such as those identified with rotor core, PM shape and armature coil slot shape. The rotor parameters are rotor radius (L1), rotor pole width (L2), and rotor pole height (L3). The PM shape parameters are PM width (L4), PM radial length (L5) while armature coil slot consist of armature coil width (L6), and armature coil height (L7), respectively.

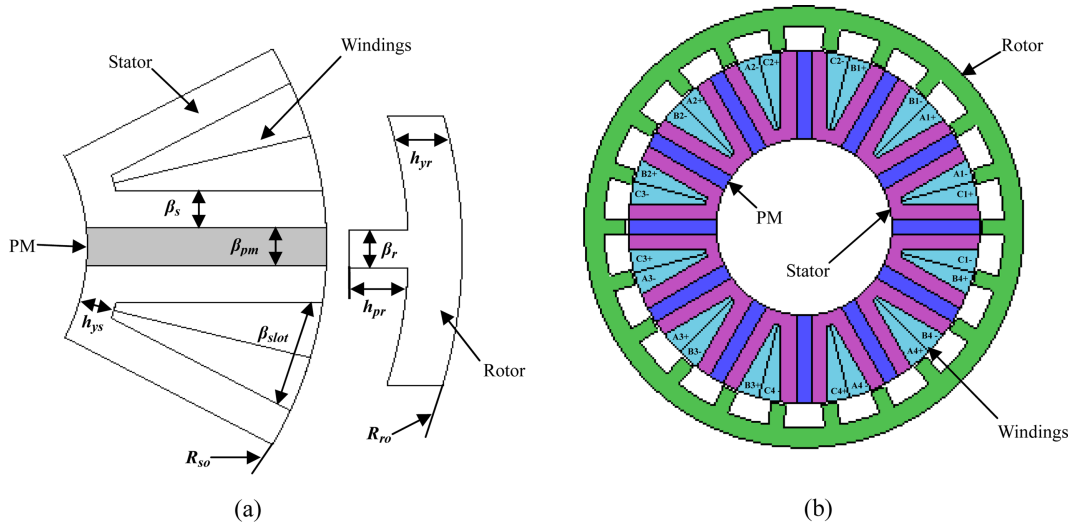

Fig. 3. (Color online) (a) Magnified local structrue (b) Complete schematic of outer rotor PMFSM.

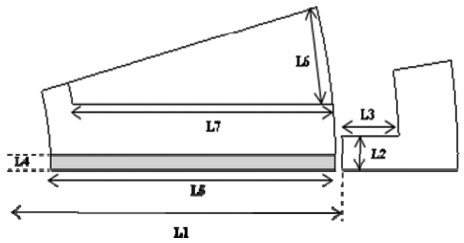

Fig. 4. Design free parameters of 12s-22p PMFSM.

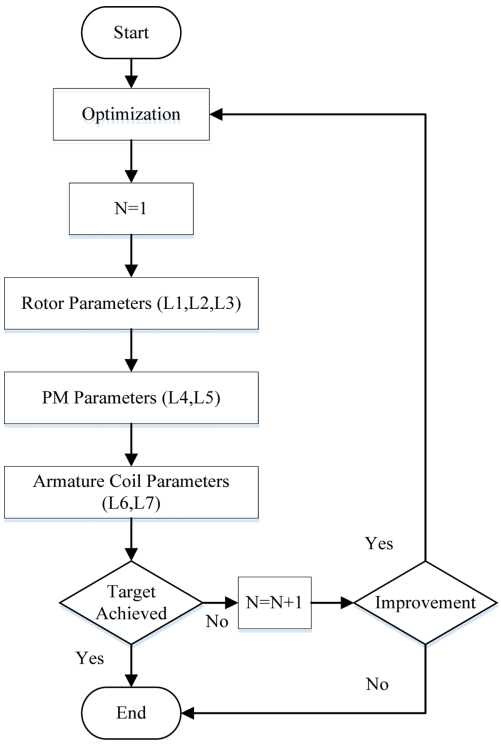

Fig. 5. (Color online) Work flow diagram of deterministic approach.

3.1. Split Ratio

In outer rotor machines, the ratio of stator external radius to rotor external radius is necessary to be improved since it fundamentally impacts torque output yield line. At initial stage, it has been fixed at 0.8, which implies the stator will possess 80 % of machine size which is valid according to outer rotor PMFSM design principle [21]. The ideal estimation of split ratio is gotten by shifting L1 while keeping all parameters consistent. This strategy rehashed for several cycles so the final value can be achieved. The maximum value of torque is accomplished when the ratio is set at 0.86 as shown in Fig. 6. In external rotor PMFSM, the larger split ratio offer completely use of stator internal space which produces higher slot area and consequently higher average torque.

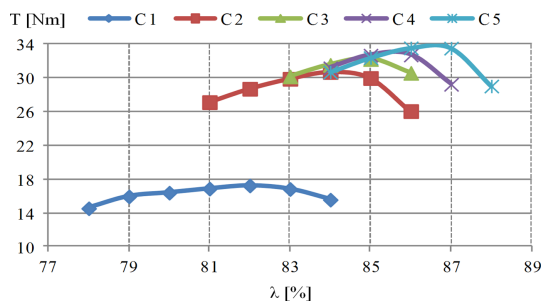

Fig. 6. (Color online) Split ratio analysis of outer rotor PMFSM.

3.2. Rotor Pole Width & Height

For concentrating the stream of flux while decreasing the vibration and windage losses in proposed design, the rotor pole width L2 and height L3 need to be refined. Initially, they are set at 3.49 mm and 5 mm respectively,

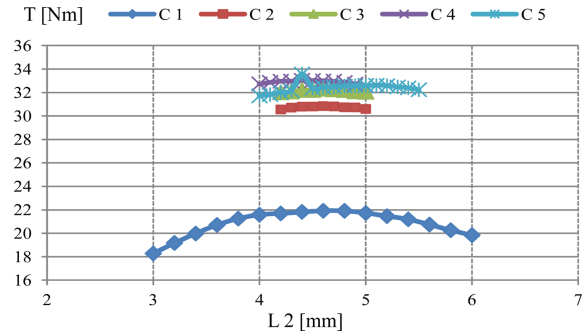

Fig. 7. (Color online) Rotor pole width versus torque investigation.

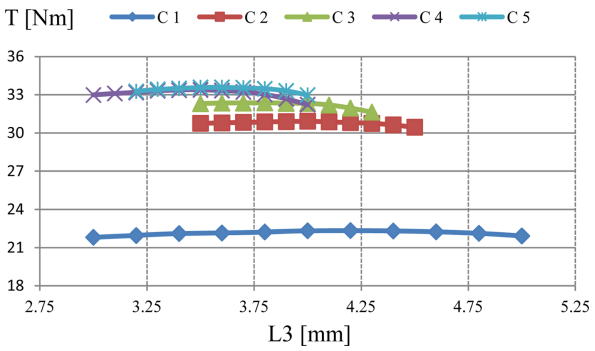

Fig. 8. (Color online) Rotor pole height variation at different cycles.

where the output torque was 16.39 Nm beneath from focused range. Hence, these two parameters should be refined with a specific end goal to improve the performance of the machine. The first step is to adjust L1 by keeping all other parameters constant. Then, L2 is modified in order to obtain the maximum value of output torque. This procedure is repeated for multiple cycles so that the best value can be achieved. By picturing Fig. 7 and 8, it can be viewed that the pinnacle yield torque is achieved after five cycles where rotor pole width and height are settled at 4.4 mm and 3.6 mm correspondingly.

3.3. Permanent Magnet Width and Radial Length

In numerous applications, high utilization of PM causes the undesirable impacts of high cogging torque that can aggravate performance of the machine. Hence it is compulsory to characterize the finest estimation of PM in machine designing. This could be possible by modifying PM width L4 while keeping other parameters constant, through deterministic approach as exhibited in Fig. 9. In basic design, the PM weight was figured around 1.26 kg. After implementation of the optimization process for several cycles, the PM length changed from 3.49 mm to 1.9 mm that decreases the weight to 0.79 kg. The next step is to adjust PM radial length L5 because it influences

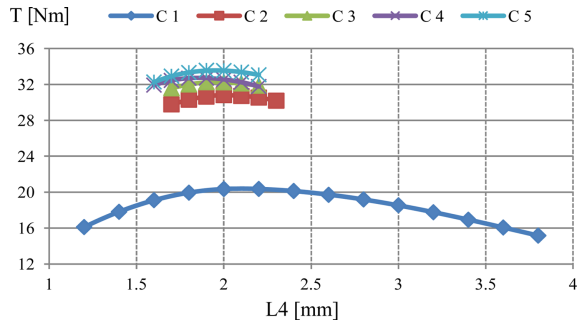

Fig. 9. (Color online) Deviation in PM width with respect to torque.

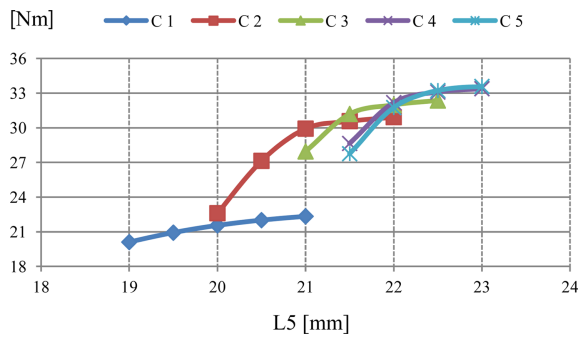

Fig. 10. (Color online) PM radial length against torque analysis.

the torque characteristics, loss, and efficiency. The radial length preliminary fixed at 19 mm, which changes to 23 mm after refinement shown in Fig. 10. The optimization of both parameters has built the electromagnetic torque.

3.4. Number of Turns

The numbers of turns play fundamental part in the enhancement of electric machine performance. Subsequently, the necessary armature slot area A_{slot} is dictated by shifting armature coil height, L6 and armature coil width, L7 to oblige whole number of turns, Na for armature loop. In the deterministic method, armature slot area parameters L6 and L7 are dealt with while keeping different parameters examined above constant. The plot of torque

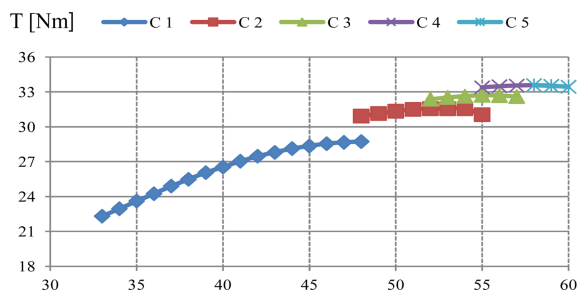

Fig. 11. (Color online) Average output torque at various number of turns.

versus Na is portrayed in Fig. 11. The maximum torque is acquired when Na is 58 turns, L6 is 13.94 mm and L7 is 21.20 mm, respectively. The increment in electromagnetic torque is mainly due more magnetic flux induced by the higher number of turns. Although, armature current density remains same but slot area has been enlarged.

4. Results & Performance Comparison

The performance correlation is completed under open circuit and close circuit. The no load examination incorporates flux linkage and distribution, cogging torque and induced voltages while load investigation consist of torque characteristic, torque-power versus speed curve, and efficiency analysis.

4.1. Flux Linkage

For initial and optimized design, the total flux in the machine is generated by PM only when the rotor is rotated at speed of 1000 rpm while the armature current density is fixed at 0 A/mm^2. From Fig. 12, in enhanced design, the u-phase flux linkage of 12s-22p has been increased to 0.2Wb which is twice of preliminary design. The flux is doubled because the rotor pole height is shortened so it means the flux will take shorter time to complete one cycle.

4.2. Flux Distribution

The objective of flux distribution is to control the stream of flux while checking the impact of flux saturation in the machine. Meanwhile, Fig. 13(a) shows that initial design experiences flux cancellation effect and leakage highlighted in red circles. After implementation of deterministic optimization technique, the leakage factor is improved from 0.75 to 0.95 while wiping out the effect of flux cancellation depicted in Fig. 13(b).

4.3. Cogging Torque

It is additionally called as detent or no-current torque that makes noise and vibration in machine operation. The PM produced cogging torque investigation for one electrical cycle is illustrated in Fig. 14. The cogging torque waveform has 6 numbers of cycles that are determined as [22]

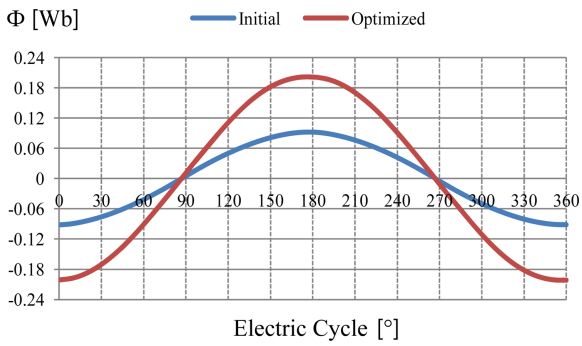

Fig. 12. (Color online) U-phase flux linkage of initial and enhanced design.

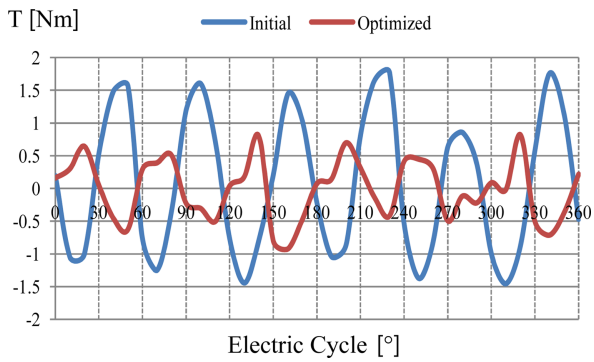

Fig. 14. (Color online) Cogging torque analysis for one electric cycle.

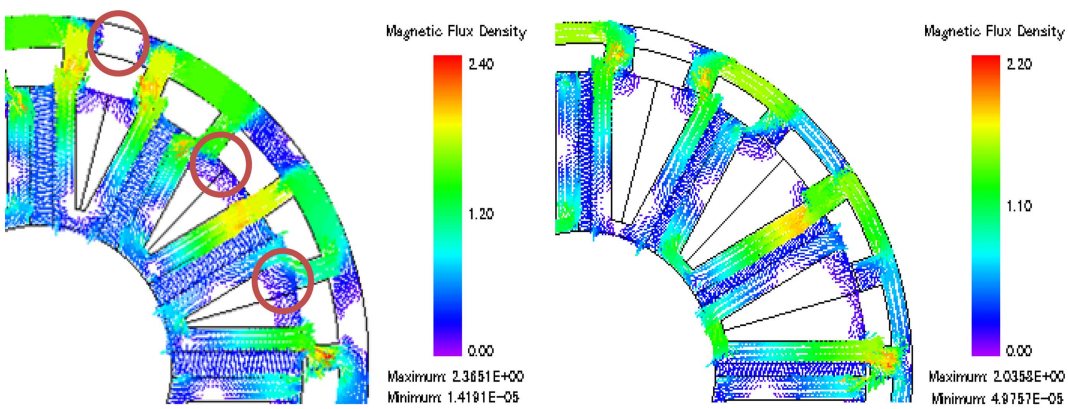

(a) (b)

Fig. 13. (Color online) Flux distribution of 12s-22p (a) Initial (b) Optimized.

$$N_p = \frac{N_r}{HCF[N_r\ N_s]} \tag{10}$$

$$N_e = \frac{N_p\ N_s}{N_r} \tag{11}$$

The preparatory design of outer rotor PMFSM for the downhole application with 12slot-22poles has high crest to crest cogging torque of around 3.2 Nm which is which is reduced to is about 1.74 Nm after optimization due to decrement in PM weight.

4.4. Induced Voltages

Further examination of the both designs on back-Emf in no load condition is carried out at the speed of 1000 rev/m. The outcomes acquired for back-Emf are plotted in Fig. 15. The improved design has higher induced voltages than the initial design in light of the fact that the induced emf (E) is directly proportional to the flux linkage (ϕ), illustrated in Eq. (12) while k is the constant value, depends on the machine geometry and ω is speed.

$$E = k\phi\omega \tag{12}$$

As flux is doubled after optimization, the induced voltages of optimized design are much higher than the initial design under load condition as shown in Fig. 16. Furthermore, induced voltages of optimized design under base and maximum speed is illustrated in Fig. 17, where magnetic flux is almost same but the speed is changed that is why maximum speed has high value of induced voltages.

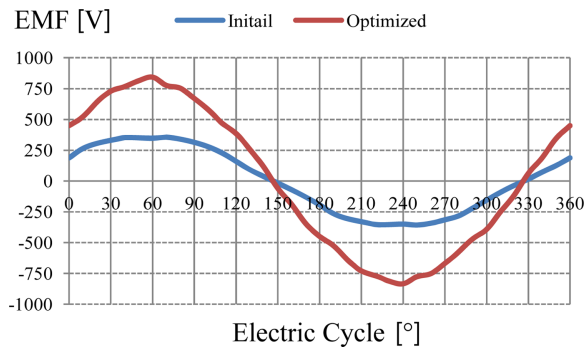

Fig. 15. (Color online) Induced voltage comparison of initial and optimized design.

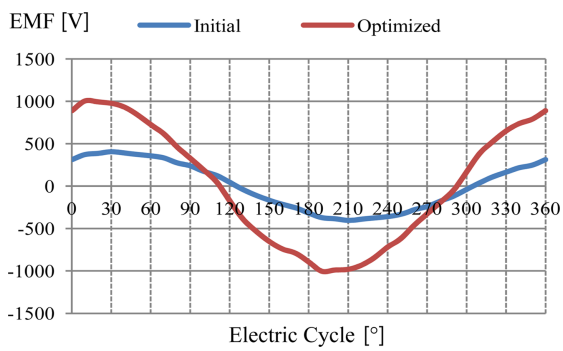

Fig. 16. (Color online) Induced voltage of initial and enhanced design under load condition.

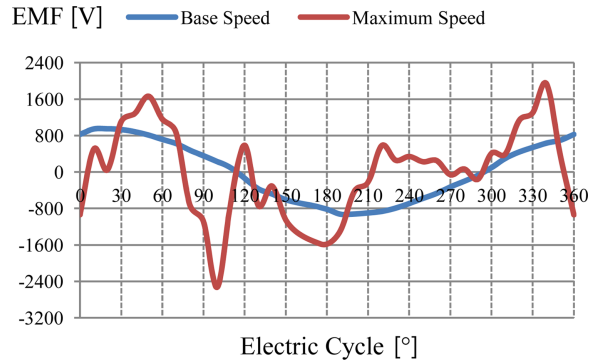

Fig. 17. (Color online) Back-emf of optimized design under base and maximum speed.

In addition, induced voltages of optimized design are greater than applied voltages but can be used for regenerative braking system in order to charge the source.

4.5. Average Output Torque at Various Armature Current Densities

The average electromagnetic torque of proposed configuration can be computed as [23]

$$T_{avg} = \frac{\pi}{8} N_r K_d B_g J_a A_{slot} R_{so} l \alpha \tag{13}$$

Where B_g is maximum air gap flux density at no load condition, K_d is leakage factor which is taken as 0.75 for initial design while for improved design it is 0.95. The obtained results from calculation and simulation are plotted in Fig. 18, in which armature current density is

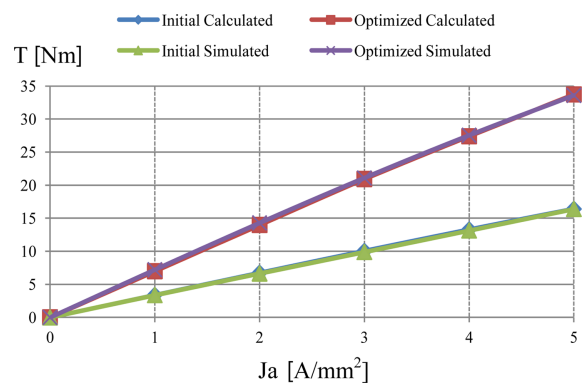

Fig. 18. (Color online) Torque analysis at different armature current densities.

varied from 0 A/mm^2 to 5 A/mm^2. For initial design, the highest calculated and simulated output torque of 16.39 Nm and 16.61 Nm were acquired at 5 A/mm^2. After design improvement, the maximum simulated and calculated torque of 33.57 Nm and 33.67 Nm respectively are obtained at 5 A/mm^2 which is approximately 51.17 % greater than initial design.

4.6. Torque-Power versus Speed Characteristic Curve

For starting and refined outer rotor PMFSM for the downhole application, the torque and power versus speed curve is plotted in Fig. 19 and 20. At the base speed 2406.55 r/min and 973.32 r/min, the maximum torque of 16.39 Nm and 33.57 Nm is obtained and torque start to decline if the machine is operated beyond the base speed. The power accomplished by preliminary and improved design is 4.13 kW and 3.84 kW respectively. The improved design has less power than initial design but it is still above the targeted value.

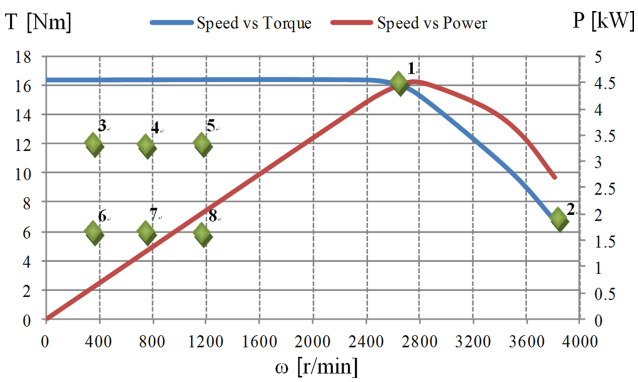

Fig. 19. (Color online) Torque-power versus speed characteristic curve of initial design.

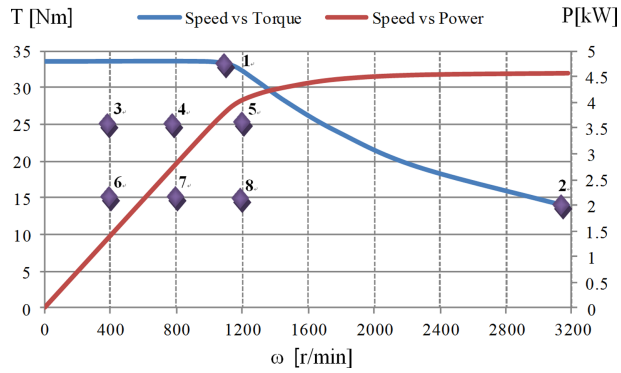

Fig. 20. (Color online) Torque and power against speed analysis for optimized design.

4.7. Machine Losses and Efficiency Predictions

The motor loss and efficiency are figured by finite element analysis considering copper losses in the armature winding and iron losses in all laminated cores. The particular operating points at maximum torque and regular operating point under light load driving condition noted as No. 1 to No. 8 are already specified in torque-power versus speed graph for initial and optimized design. Meanwhile, the detail losses investigation and motor efficiencies of the initial and improved design are summarized in Table 3 accordingly. In particular, point 1 and 2 represents the maximum operating torque and speed of both designs whereas point 3 up to point 8 falls under the similar average operating region of initial and optimized design.

Table 3. Specifications of initial outer rotor PMSFM for the downhole application.

Machine Designs	Operat. Points	Speed (r/min)	Output Power (kW)	Iron Loss (kW)	Copper Loss (kW)	Eff. (%)
Initial	1	2406.5	4.13	0.20	0.05	94.08
	2	3809.3	2.69	0.29	0.05	88.45
	3	400	0.50	0.01	0.03	91.22
	4	800	1.00	0.03	0.03	93.57
	5	1200	1.50	0.06	0.03	93.93
	6	400	0.25	0.01	0.009	92.15
	7	800	0.50	0.03	0.009	92.10
	8	1200	0.75	0.06	0.009	91.17
Optimized	1	973.3	3.42	0.08	0.10	95.02
	2	3175.9	4.58	0.12	0.10	95.33
	3	400	1.04	0.01	0.06	93.09
	4	800	2.09	0.03	0.06	95.37
	5	1200	3.14	0.08	0.06	95.57
	6	400	0.62	0.01	0.03	93.09
	7	800	1.25	0.02	0.03	95.07
	8	1200	1.88	0.04	0.03	95.41

Table 4. Overall performance comparison of initial and optimized design.

Items	Initial	Optimized
Torque (Nm)	16.39	33.57
Power (kW)	4.1	4.5
Speed (r/min)	3809.3	3175.9
Output power (kW)	11.34	18.05
Iron losses (kW)	0.71	0.42
Copper losses (kW)	0.25	0.50
Efficiency (%)	92.08	94.74

At each design's base speed where highest torque is accomplished, the optimized machine gives off an impression of being the most astounding productivity with 94.74 % in spite of the fact that it has the most copper losses, trailed by initial machine design with 92.08 %. Besides this, while running at the normal operating points, the maximum efficiency is acquired for optimized design at point 5 with the consequence of 95.57 %. The summarized performances of both machine designs are outlined in Table 4.

5. Conclusion

This paper has introduced the design modeling and performance analysis of outer rotor PMFSM for the downhole application. The optimization technique has been clearly described for the accomplishment of focused performance. As an outcome, the proposed machine has better torque, efficiency and low cogging torque when contrasted with the initial design. The optimized machine design has enhanced approximately 51.17 % of maximum torque while lessening the PM weight by 37.3 %. The diminishment in PM weight makes machines lighter and simple to manufacture. Finally, it can be concluded with all the analytical study that optimized design of outer rotor PMFSM is one of the prominent candidates for the downhole application.

Acknowledgement

This research work was promoted by Research, Innovation, Commercialization and Consultancy (ORICC) UTHM, Batu Pahat under Vot number U519 and Ministry of Higher Education Malaysia (MOHE).

References

[1] World Energy Outlook, International Energy Agency (2013) pp. 63.
[2] Oil and Gas Industries Technology Master Plan, European Oil and Gas Innovation Forum (2004) pp. 4.
[3] I. Sandrea and R. Sandrea, Oil and Gas Journal (2007) pp. 1-8.
[4] A. Chen, R. B. Ummaneni, R. Nilssen, and A. Nysveen, 13th International Power Electronics and Motion Conference, Poland (2008) pp. 814-818.
[5] N. Griffiths and S. Breit, 35th Workshop on Geothermal Reservoir Engineering, USA (2010).
[6] A. Chen, Ph.D Thesis, Norwegian University of Science and Technology, Norway (2011) pp. 1-141.
[7] A. Chen, R. Nilssen, and A. Nysveen, IEEE Trans. Ind. Appl. **46**, 779 (2010).
[8] M. Solesa and V. Sagalovskiy, MEALF, Oman (2007).
[9] Z. Bingyi, L. Bingxue, F. Guihong, and Z. Fuyu, IEEE International Conference on Mechatronics and Automation, China (2007) pp. 1011-1016.
[10] S. E. Rauch and L. J. Johnson, AIEE Trans. Power Appl. Sys. **74**, 1261 (1995).
[11] E. Hoang, A. H. B. Ahmed, and J. Lucidame, Switching Flux PM Polyphased Synchronous Machines, 7th European Conference on Power Electronics Applications **3**, 903 (1997).
[12] Z. Q. Zhu, Y. Pang, D. Howe, S. Iwasaki, R. Deodhar, and A. Pride, IEEE Trans. Magn. **41**, 4277 (2005).
[13] C. S. Walter, H. Polinder, and J. A. Ferreira, IEEE Journal of Emerging and Selected Topics in Power Electronics **1**, 327 (2013).
[14] Z. Q. Zhu, J. T. Chen, and D. Howe, IEEE Trans. Magn. **44**, 4313 (2008).
[15] M. Jenal, E. Sulaiman, M. Z. Ahmad, F. Khan, and M. F. Omar, XXII International Conference on Electrical Machines, Switzerland (2016) pp. 2399-2405.
[16] C. V. Aravind, M. Norhisam, I. Aris, D. Ahmad, and M. Nirei, IEEE SCORED, Malaysia (2011) pp. 294-299.
[17] W. Xu, J. Zhu, Y. Zhang, Y. Wang, Y. Li, and J. Hu, 20th Australian Universities Power Engineering Conference (2010).
[18] M. Jenal, E. Sulaiman, and R. Kumar, J. Magn. **21**, 537 (2016).
[19] M. Jenal, E. Sulaiman, F. Khan, and Md. Z. Ahmad, Applied Mechanics and Materials **785**, 274 (2015).
[20] W. Fei, P. C. K. Luk, J. X. Shen, Y. Wang, and M. Jin, IEEE Trans. Ind. Appl. **48**, 1496 (2012).
[21] R. Kumar, E. Sulaiman, F. Khan, L. I. Jusoh, and F. S. Bahrim, 2nd International Conference on Science and Technology for Sustainability (2016).
[22] A. Zulu, Ph.D Thesis, Newcastle University, United Kingdom (2010).
[23] J. X. Shen, Y. Wang, C. F. Wang, W. Z. Fei, and P. C. Luk, The International Journal for Computation and Mathematics in Electrical and Electronic Engineering **30**, 48 (2011).